Article

Imaging and Quantification of Isotachophoresis Zones Using Nonfocusing Fluorescent Tracers

Robert D. Chambers, and Juan G. Santiago

Anal. Chem., **2009**, 81 (8), 3022-3028• DOI: 10.1021/ac802698a • Publication Date (Web): 16 March 2009

Anal. Chem. **2009,** *81,* 3022–3028

Imaging and Quantification of Isotachophoresis Zones Using Nonfocusing Fluorescent Tracers

Robert D. Chambers and Juan G. Santiago*

Department of Mechanical Engineering, Stanford University, Stanford, California 94305

We present a novel method for visualizing isotachophoresis (ITP) zones. We introduce negligibly small concentrations of a fluorophore that is not focused by isotachophoresis. This nonfocusing tracer (NFT) migrates through multiple isotachophoresis zones. As it enters each zone, the NFT concentration adapts to the local electric field in each zone. ITP zones can then be visualized with a point detector or camera. The method can be used to detect, identify, and quantify unknown analyte zones and can visualize complex and even transient electrophoresis processes. This visualization technique is particularly suited to microfluidic and laboratory-on-a-chip applications, as typical fluorescence microscopes and charge-coupled device (CCD) cameras can provide high-resolution spatiotemporal data. We present a theoretical description, a methodology for identifying analytes, and experimental validation. We also visualize and analyze a complex, transient DNA ITP preconcentration and separation.

Isotachophoresis (ITP) is an established technique for analyte preconcentration and separation in which ions form discrete and contiguous zones between a fast leading electrolyte (LE) and a slow trailing electrolyte (TE). Its applications,[1] theory,[2] and relation to other electrophoresis techniques[3] have been reviewed in detail elsewhere, and there are over 2300 articles on the subject. Much of the work falls into two categories: design of electrolyte systems for separations and methods to detect separated analytes. We here address the latter.

Analyte detection methods in ITP are either direct or indirect. Direct methods sense analyte molecules with (typically) UV absorbance, electrochemical, or fluorescence detection. Indirect methods sense surrogate physicochemical phenomena (e.g., local temperature or electric field) affected by the analyte.[4] Analytes have been indirectly detected through quenching of a fluorophore in micellar electrokinetic capillary electrophoresis[5] and through displacement of UV- or fluorescence-detectable background ions in capillary electrophoresis (CE).[6−8] Recently, Khurana and Santiago described a detection scheme which detects ITP analyte zones indirectly by imaging "gaps" in the signal of fluorescent mobility markers.[9] Fluorescence-based methods are particularly suited to on-chip applications, as on-chip channels offer excellent optical access but often small optical path lengths.[10]

In this paper, we describe a novel method for indirectly detecting analytes in ITP, and for general monitoring of ITP processes. We add a fluorescent nonfocusing tracer (NFT) to the LE or TE in concentrations which do not significantly affect zones' electric fields. The tracer does not isotachophoretically focus, and instead migrates through all zones, adapting its concentration in each.[11] The method can monitor ITP distributions in time and space.

THEORY

Sample injection strategies for ITP are varied and include mixing sample uniformly with TE[12] or, more commonly, injecting sample ions between the TE and LE.[9,13] We here concentrate on the latter. At steady state, LE, sample, and TE ions arrange themselves into a contiguous train of ions which electromigrate at equal velocities. The effective mobility of ions typically decreases monotonically from LE to TE, but such ordering is not required.[14] In finite sample injections, steady-state sample zones can be classified as either peak or plateau mode. Peak mode is characterized by low initial sample amounts and approximately Gaussian distributions whose shape is determined by the distribution of adjacent ions.[15,16] Plateau mode is characterized by larger injection amounts and saturated, locally uniform concentration profiles bounded by diffuse boundaries with adjacent ions.[17]

* To whom correspondence should be addressed. E-mail: juan.santiago@stanford.edu. Fax: 650-723-7657.

(1) Gebauer, P.; Mala, Z.; Bocek, P. *Electrophoresis* **2007**, *28*, 26–32.
(2) Everaerts, F. M.; Beckers, J. L.; Verheggen, T. P. E. M. *Isotachophoresis: Theory, Instrumentation, And Applications*; Elsevier Scientific Publishing Co.: Amsterdam, New York, 1976.
(3) Beckers, J. L.; Bocek, P. *Electrophoresis* **2000**, *21*, 2747–2767.
(4) Vacik, J.; Zuska, J. *J. Chromatogr.* **1974**, *91*, 795–808.
(5) Bailey, C. G.; Wallenborg, S. R. *Electrophoresis* **2000**, *21*, 3081–3087.
(6) Foret, F.; Fanali, S.; Ossicini, L.; Bocek, P. *J. Chromatogr.* **1989**, *470*, 299–308.
(7) Hjerten, S.; Elenbring, K.; Kilar, F.; Liao, J. L.; Chen, A. J. C.; Siebert, C. J.; Zhu, M. D. *J. Chromatogr.* **1987**, *403*, 47–61.
(8) Kuhr, W. G.; Yeung, E. S. *Anal. Chem.* **1988**, *60*, 2642–2646.
(9) Khurana, T. K.; Santiago, J. G. *Anal. Chem.* **2008**, *80*, 279–286.
(10) Gotz, S.; Karst, U. *Anal. Bioanal. Chem.* **2007**, *387*, 183–192.
(11) Our NFT technique is significantly different from the traditional use of background ions as tracers. In traditional indirect fluorescence applications, fluorescent (or strongly UV absorbing) background ions are present in sufficiently high concentration that they are displaced by the constraints of conservation of current and net neutrality. In contrast, the NFTs we employ here are present in negligible concentration, contribute negligibly to current, and consequently have concentration profiles which differ substantially from those of background ions.
(12) Jung, B.; Bharadwaj, R.; Santiago, J. G. *Anal. Chem.* **2006**, *78*, 2319–2327.
(13) Prest, J. E.; Baldock, S. J.; Fielden, P. R.; Goddard, N. J.; Brown, B. J. T. *J. Chromatogr., A* **2003**, *990*, 325–334.
(14) Gebauer, P.; Bocek, P. *J. Chromatogr.* **1983**, *267*, 49–65.
(15) Gebauer, P.; Bocek, P. *Electrophoresis* **1995**, *16*, 1999–2007.
(16) Svoboda, M.; Vacik, J. *J. Chromatogr.* **1976**, *119*, 539–547.
(17) Chen, S. J.; Graves, S. W.; Lee, M. L. *J. Microcolumn Sep.* **1999**, *11*, 341–345.

10.1021/ac802698a CCC: $40.75
Published on Web 03/16/2009

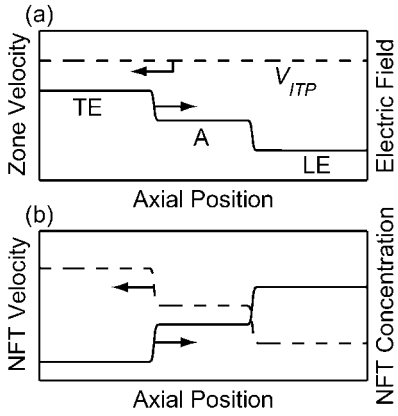

Figure 1. Qualitative representation of ITP and the adaption of a nonfocusing tracer (NFT). In steady state, all zones travel at the same velocity V_{ITP}. If the effective mobilities of the trailing (TE), analyte (A), and leading (LE) ions are such that $\bar{\mu}_{TE} < \bar{\mu}_A < \bar{\mu}_{LE}$, then the electric field must follow $E_{TE} > E_A > E_{LE}$, as shown in panel a. If the NFT has the same effective mobility in each zone, then by continuity and eq 1 its concentration must adapt, as in panel b. Consequently, zones can be indirectly detected by measuring the tracer concentration.

ITP theory is reviewed elsewhere,[2,18,19] and we present a brief analysis of NFT signals. The ITP process and distributions of an NFT are shown qualitatively in Figure 1 (an LE, single analyte, and TE). The tracer is a fluorescent species which does not meet ITP focusing conditions.[14] We classify NFTs into three categories.[20] The first, which we term *counterspeeders*, are counterionic tracers (sign of valence opposite to sample). The second, fast coionic tracers (*overspeeders*), have higher effective mobilities than focused ions in each zone and so electromigrate from TE to LE without focusing. The third, slow coionic tracers (*underspeeders*), have lower effective mobilities than focused ions in each zone and move from the LE zone to the TE zone. We recommend counterspeeders for most applications (see below).

As shown in Figure 1, the velocity of any species i in zone A is related to the electric field E_A by its local effective mobility $\bar{\mu}_{i,A}$:

$$V_{i,A} = \bar{\mu}_{i,A} E_A \tag{1}$$

Here, lowercase subscripts refer to chemical species, and uppercase subscripts refer to the ITP plateau zone in which a quantity is evaluated. As a special case, zones are named after focused analytes, so $V_{a,A}$ is the velocity of focused a ions in zone A.

A monovalent acid or base's effective mobility is governed by its limiting fully ionized mobility μ_i, and the fraction $f_{i,A}$ of its molecules which are ionized (expressed in terms of its acid dissociation constant, pK_a, and local pH), both functions of local ionic strength.[21−24] For a monovalent acid in a zone A we write

$$\bar{\mu}_{i,A} = \mu_{i,A} f_{i,A} = \mu_{i,A} \frac{1}{1 + 10^{(pK_a)_i - pH_A}} \tag{2}$$

At steady state and in a reference frame moving at the ITP velocity[2] V_{ITP}, ionic fluxes of all species, $c_i V_i$, are equal at any point. For focused ions, these fluxes are zero. For nonfocused ions, balancing the flux of a species i between two zones (here, A and L) yields the ratio of its concentration in those zones:

$$\frac{c_{i,A}}{c_{i,L}} = \frac{V_{i,L} - V_{ITP}}{V_{i,A} - V_{ITP}} \tag{3}$$

Combining with eq 1, the concentration ratio can be cast in terms of the effective mobilities of the NFT species i and the two focused species a and l:

$$\frac{c_{i,A}}{c_{i,L}} = \frac{\bar{\mu}_{a,A}}{\bar{\mu}_{l,L}} \frac{\bar{\mu}_{i,L} - \bar{\mu}_{l,L}}{\bar{\mu}_{i,A} - \bar{\mu}_{a,A}} \quad \text{(general case)} \tag{4}$$

The effective mobilities that determine $c_{i,A}/c_{i,L}$ can, in many cases, be calculated analytically.[2,19] Alternatively, numerical codes can conveniently determine the ratio, and take into account ionic strength effects and multiple nonfocused analytes (see the Simulations section, below). If the tracer signal is proportional to its concentration (e.g., concentrations which do not self-quench),[25] then the ratio of the signal intensity in a sample zone, I_A, to that in the leading zone, I_L, is

$$\frac{I_A}{I_L} = \frac{\bar{\mu}_{a,A}}{\bar{\mu}_{l,L}} \frac{\bar{\mu}_{i,L} - \bar{\mu}_{l,L}}{\bar{\mu}_{i,A} - \bar{\mu}_{a,A}} \quad \text{(tracer intensity ratio)} \tag{5}$$

For the special case of a fully ionized, high-mobility counterspeeder, this ratio approaches that of the focused ions' mobilities:

$$\frac{I_A}{I_L} \approx \frac{\bar{\mu}_{a,A}}{\bar{\mu}_{l,L}} \quad \text{(counterspeeder approximation)} \tag{6}$$

For coionic tracers, the most sensitive regimes are where $\bar{\mu}_{i,A} \approx \bar{\mu}_{a,A}$, and the least sensitive regimes are where $\bar{\mu}_{i,L} \approx \bar{\mu}_{l,L}$ (sensitivity is further discussed in the Supporting Information). In the Results and Discussion section we validate this analysis with examples.

Application to Analyte Detection and Identification. Even for a given NFT and analyte, the tracer intensity ratio I_A/I_L depends strongly on the composition of the LE. Figure 2 shows the effect of three LE chemistries (LE_1, LE_2, and LE_3) on contours of I_A/I_L (from eq 5) for a counterspeeder rhodamine 6G (R6G) in analyte zone A. In Figure 2a, both LEs contain 200 mM of fully ionized leading ion (chloride) and 267 mM of counterion, but LE_2 contains a counterion with higher pK_a. Figure 2b shows the effect of adding 100 mM NaOH to LE_1 (which we term LE_3).

When an analyte's pK_a is lower than that of the counterion(s), I_A/I_L is primarily a function of analyte mobility; at higher analyte pK_a, both mobility and pK_a are relevant. Most interestingly, I_A/I_L may differ markedly depending on the LE counterion(s), even for the same analyte. We hypothesize that multiple LEs with markedly different contour slopes in the vicinity of an analyte's mobility and pK_a are especially useful in determining species'

(18) Bocek, P. *Analytical Isotachophoresis*; VCH: Weinheim, Cambridge, 1987.
(19) Schafernielsen, C.; Svendsen, P. J.; Rose, C. *J. Biochem. Biophys. Methods* **1980**, *3*, 97–128.
(20) Although tracers are typically nonfocusing in the entire ITP domain, the current theory applies also to tracers which may traverse several zones, but then focus at a subsequent interface.
(21) Davies, C. W. *J. Chem. Soc.* **1938**, 2093–2098.
(22) Sun, M. S.; Harriss, D. K.; Magnuson, V. R. *Can. J. Chem.* **1980**, *58*, 1253–1257.
(23) Porras, S. P.; Riekkola, M. L.; Kenndler, E. *Electrophoresis* **2003**, *24*, 1485–1498.
(24) Robinson, R. A.; Stokes, R. H. *J. Am. Chem. Soc.* **1954**, *76*, 1991–1994.
(25) Arbeloa, F. L.; Ojeda, P. R.; Arbeloa, I. L. *J. Chem. Soc., Faraday Trans. 2* **1988**, *84*, 1903–1912.

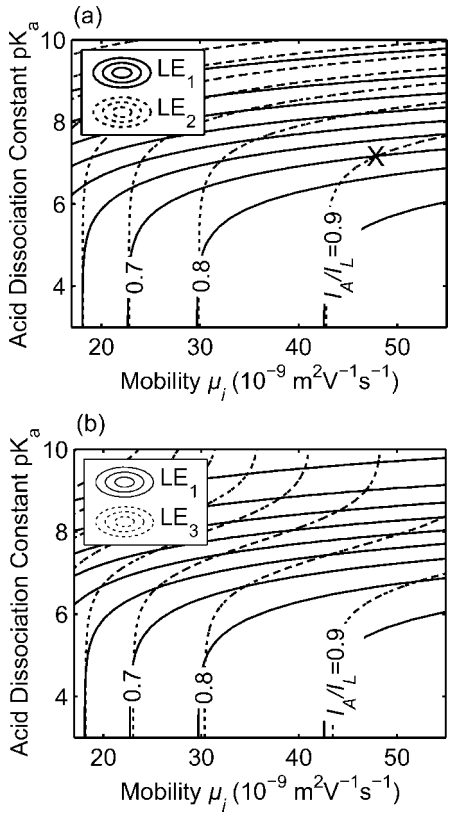

Figure 2. Contour plots of the ratio of tracer intensity in an analyte zone to that in an LE (I_A/I_L), for several LEs. Each LE contains chloride and a weak monovalent base, and I_A/I_L is calculated for monovalent acids with varying mobilities and pK_a's. In plot a, LE_1 and LE_2 contain counterions with different pK_a's. The point marked "X" represents an analyte whose mobility and pK_a can be determined by ITP experiments with LE_1 and LE_2 (see text). In plot b, LE_3 is similar to LE_1 but also contains 100 mM NaOH, producing markedly different contours. All LEs contained 200 mM chloride and 50 μM R6G, but each contained different types or amounts of buffering counterion: LE_1, 267 mM BisTris, pH 6.0; LE_2, 267 mM Tris, pH 7.6; LE_3, 267 mM BisTris and 100 mM NaOH, pH 6.7.

identities. Multiple observations have the potential to achieve a two-dimensional assay functionality, sensitively measuring both mobility and pK_a. As an example, we show in Figure 2a an analyte (marked by an "X") which yields $I_A/I_L = 0.7$ with LE_1, but 0.9 with LE_2. Such an analyte must have pK_a and mobility of ~7.3 and ~48×10^{-9} m^2 V^{-1} s^{-1}, respectively (assuming it is a monovalent acid). This method is analogous to analyte mobility and pK_a identification via ITP with conductivity measurements.[26−28]

Peak Mode and Transient ITP. In (full or partial) peak mode[29] ITP, NFTs can be used to visualize zones in plateau mode (e.g., the TE and LE) to identify focusing regions, etc. The analysis above applies to steady state, but the method can also be used to analyze unsteady processes, as local NFT intensities are intimately related to local electric fields. We here will show an example visualization of a transient ITP assay.[30] In all cases, NFT visualizations can be used to validate numerical simulations, by comparing predicted and measured intensity profiles.

Table 1. Selected Fully Ionized Mobilities [m^2 V^{-1} s^{-1}] and pK_a's

chemical name	(valence, mobility × 10^9)	pK_a
acetic acid	(−1, 42.4) (ref 27)	4.756 (ref 27)
$Ba(OH)_2$	(+2, 66) (ref 31)	strong base (ref 31)
BisTris	(+1, 26) (ref 31)	6.46 (ref 31)
chloride	(−1, 79.1) (ref 28)	strong acid (ref 28)
glycine	(+1, 39.5), (−1, 37.4) (ref 45)	2.32, 9.78 (ref 45)
HEPES	(−1, 21.8) (ref 26)	7.5 (ref 26)
MES	(−1, 26.8) (ref 26)	6.13 (ref 26)
MOPS	(−1, 24.4) (ref 26)	7.16 (ref 26)
tricine	(−1, 26.6) (ref 28)	8.15 (ref 28)
Tris	(−1, 29.5) (ref 27)	8.076 (ref 27)

EXPERIMENTAL SECTION

Materials and Instrumentation. For the steady-state ITP experiments, we visualized plateau zones with either cationic R6G (Acros Organics, Geel, Belgium) or anionic Alexa Fluor 488 succinimidyl ester (Molecular Probes, Eugene, OR). For the transient ITP experiments, we visualized a DNA ladder ranging from 100 to 1517 base pairs (no. n3231 from New England Biolabs, Ipswich, MA) using the cationic intercalating dye SYBR Green (Molecular Probes, Eugene, OR). Stock solutions of fluorophores and DNA were split into aliquots and frozen to prevent degradation. Buffers were prepared in deionized ultrafiltered water (DIUF) from Fischer Scientific (Pittsburgh, PA). We suppressed electroosmotic flow (EOF) with ~1 MDa poly(vinylpyrrolidone) (PVP) (Polysciences Inc., Warrington, PA). All other chemicals were obtained from Sigma-Aldrich (St. Louis, MO). The pH values we report throughout this paper were predicted numerically (see the Simulations section, below) using the pK_a values listed in the Table 1; these pH values were found to be in excellent agreement with measured pH.

We used off-the-shelf microfluidic borosilicate chips (model NS-95) from Caliper Life Sciences (Mountain View, CA). The channels are a simple cross geometry and wet-etched to a 12 μm depth. Channels consist of narrow (10 μm mask width) separation regions which expand to wider (50 μm mask width) injection regions. We performed experiments in either potentiostatic mode with a computer-controlled Labsmith HVS-3000D high-voltage sequencer (Livermore, CA), or galvanostatic mode with a Keithley 2410 high-voltage sourcemeter (Keithley Instruments, Cleveland, Ohio). We used a custom (inclined tube) adjustable-height water column (from −6 to 6 kPa) and/or a vacuum pump to adjust pressure in the wells.

We monitored the ITP process with an IX70 inverted fluorescence microscope equipped with 5× (NA of 0.1) and 10× (NA of 0.4) objectives and a model U-MWIBA filter cube (460−490 nm excitation, 515 nm emission), all from Olympus (Hauppauge, NY). Images were captured with a 12-bit 1300 by 1030 pixel charge-coupled device (CCD) camera (fx16 Coolsnap; Roper Scientific, Trenton, NJ) controlled with open source μManager microscopy

(26) Pospichal, J.; Gebauer, P.; Bocek, P. *Chem. Rev.* **1989**, *89*, 419–430.
(27) Hirokawa, T.; Nishino, M.; Aoki, N.; Kiso, Y.; Sawamoto, Y.; Yagi, T.; Akiyama, J. *J. Chromatogr.* **1983**, *271*, D1–D106.
(28) Marak, J.; Nagyova, I.; Kaniansky, D. *J. Chromatogr., A* **2003**, *1018*, 233–249.
(29) Khurana, T. K.; Santiago, J. G. *Anal. Chem.* **2008**, *80*, 6300–6307.
(30) Xu, Z. Q.; Nishine, T.; Arai, A.; Hirokawa, T. *Electrophoresis* **2004**, *25*, 3875–3881.
(31) Hrusca, V.; Jaros, M.; Gas, B. *Electrophoresis* **2006**, *27*, 984–991.

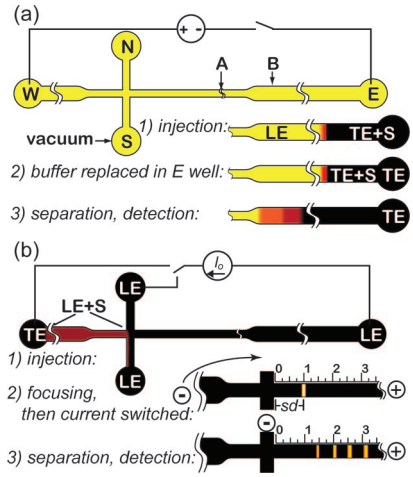

Figure 3. ITP injection protocols. For all experiments, we first flushed with LE for 5 min. For validation experiments (a), we then (1) pulled sample in TE (TE + S) into the injection region using vacuum on the S well, (2) switched the TE + S with pure TE, and applied voltage between the W and E wells. The focused zones were imaged (3) at either point A, for precise quantification of zone lengths and intensities, or in the injection region (point B) for images showing multiple analyte zones. Our transient ITP (tITP) protocol is depicted in panel b. We (1) injected sample in LE (LE + S) using vacuum on S, replaced the W well with TE, and applied constant current between the W and E well. When the ITP interface reached a designated switching distance (sd), we switched (2) the current to N. LE ions then oversped TE ions in the E channel, disrupting ITP, and initiating separation (3) of analytes.

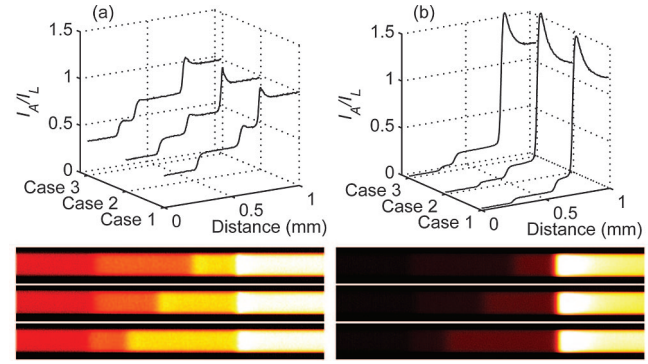

Figure 4. Detection of HEPES and MOPS with a counterionic (a) and overspeeding coionic (b) fluorescent nonfocusing tracer. Top panes are ratios of zone intensities I_A/I_L, and bottom panes are corresponding images. The zones are, from left to right, TE (tricine), HEPES, MOPS, and LE (MES). The concentration of the tracer increases in high-mobility zones. The mobility of the coionic tracer Alexa Fluor 488 (AF488) is close to that of MES, so it is especially sensitive in this region. The sensitivity of the counterionic tracer rhodamine 6G (R6G) is more uniform. LE: 100 mM MES, 200 mM BisTris, 2 mM $Ba(OH)_2$, 0.4% PVP, pH 6.6. TE: 100 mM tricine, 20 mM $Ba(OH)_2$, 0.4% PVP, pH 7.7. For the left plots, the LE contains 50 μM R6G. For the right plots, the TE contains 5 μM AF488. Voltage was 300 V. Concentrations of injected HEPES and MOPS were 9 and 3 mM (case 1), 6 mM each (case 2), or 3 and 9 mM (case 3), respectively.

software (micro-manager.org). Images were postprocessed with custom MATLAB scripts.

Assay Protocols. In all experiments, we performed repeatable length, hydrodynamic injection of analytes followed by isotachophoretic focusing and fluorescence detection, as described in Figure 3. Additionally, we cleaned channels with 0.5 M NaOH, 100 mM HCl, and DIUF between experiments (see the Supporting Information for more details).

Simulations. We used numerical codes to predict the composition, pH, and fluorescence intensity of each zone for assay design and theory validation. Transient and steady-state problems can be simulated with programs such as Simul 5[31] or a MATLAB-based program (Spresso) developed by our group.[32] For fast solution of most problems, however, we used a steady-state solver written in-house based on the RFQ method described by Beckers and Everaerts.[2,33] This code adjusts pK_a and ion mobility for ionic strength based on the Davies equation[21,22] and Robinson−Stokes model,[23,24] respectively. See Table 1 for the limiting electrophoretic mobilities and pK_a's of example chemicals used in simulations.

RESULTS AND DISCUSSION

Analyte Detection and Quantification with a Nonfocusing Tracer. In this section, we present examples of the use of NFTs to measure the mobility ranges and concentrations of nonfluorescent analytes. For this validation study, we chose well-known analytes with well-characterized properties, summarized in Table 1. In Figure 4a, we show a counterspeeding tracer, R6G, migrating from LE to TE. The tracer clearly shows the presence, width, and tracer intensities of two analyte zones. In Figure 4b, the LE, TE, and analytes are identical to those of Figure 4a, but we here used an overspeeding coionic tracer (Alexa Fluor 488) which migrates from the TE to the LE. For the counterspeeder case (Figure 4a), measured values of I_A/I_L for the three HEPES and three MOPS zones each differed by less than 2.4% of their average values. In contrast, the variation of I_A was consistently greater (variation of 10% for the HEPES zones of Figure 4b) than the variation of I_A/I_L. We therefore advocate the use of I_A/I_L for the identification of ions as this ratio helps normalize for variations associated with experimental factors such as changes in imaging conditions.

As discussed in the Theory section, the sensitivity of counterspeeders tends to be approximately uniform for all analyte mobilities. In contrast, underspeeders and overspeeders offer the potential advantage of extreme sensitivity to analytes with mobilities approximately equal to that of the tracer. In Figure 4, parts a and b, we estimate the effective mobility of the LE (MES) to be -17.8×10^{-9} m^2 V^{-1} s^{-1}, and the effective mobilities of MOPS, HEPES, and tricine to be, respectively, 58%, 41%, and 30% of that value. For the counterspeeder of Figure 4a, the ratios of analyte-to-LE zone intensities are similar to the effective mobility ratios for MOPS, HEPES, and tricine (I/I_L values of 0.69, 0.51, and 0.34, respectively). In the overspeeding case of Figure 4b, the respective values are strongly skewed: 0.18, 0.07, and 0.02. The overspeeder is extremely sensitive to the LE−MOPS boundary but is a less versatile tracer. Similar to the latter case (not shown), an underspeeder with an effective mobility of -2.5×10^{-9} m^2 V^{-1} s^{-1} (about half that of the TE) would yield respective approximate values of 1.15, 1.35, and 1.71.

Practical considerations also strongly affect the choice of tracers. For instance, with anionic ITP, the valence of a counterspeeder is often opposite to that of the (e.g., glass) wall charge and may yield problems with dye adsorption (particularly at ionic strength below about 15 mM). On the other hand, the requirement

(32) Bercovici, M.; Lele, S. K.; Santiago, J. G. *J. Chromatogr., A* **2008**, *1216*, 1008–1018.
(33) Beckers, J. L.; Everaerts, F. M. *J. Chromatogr., A* **1972**, *68*, 207–230.

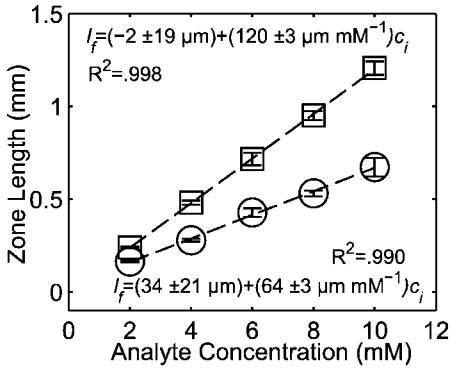

Figure 5. Length of a focused zone (here, MOPS) is proportional to the concentration of injected analyte but varies with LE. The top points (squares) are lengths of zones focused behind a low-concentration LE (lc-LE), while bottom points (circles) are behind a high-concentration LE (hc-LE). Dashed lines are linear fits. lc-LE: 100 mM acetic acid, 200 mM BisTris, 50 μM R6G, and 0.2% PVP, pH 6.5. hc-LE: 200 mM acetic acid, 400 mM BisTris, 50 μM R6G, and 0.2% PVP, pH 6.5. TE: 70 mM HEPES, 10 mM $Ba(OH)_2$, and 0.2% PVP, pH 6.8. Voltage was 700 V. Error bars represent 95% confidence intervals on the means, and $N = 4$ for each condition.

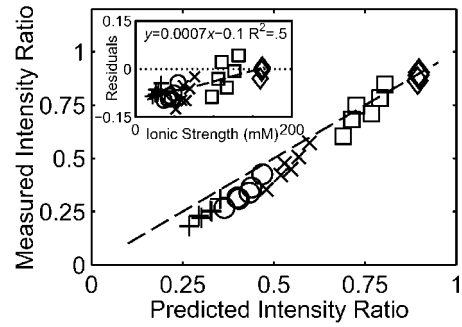

Figure 6. Experimentally measured tracer intensity ratios of analyte zones to leading zones, compared with ratios predicted numerically. Data from five analytes focusing behind six LEs are shown. General trends are well-captured but diverge somewhat for slow analytes. (The inset shows residual error between measured and predicted intensity ratios, compared with ionic strength along with a linear fit; see text.) LE: 200 mM of either acetic or hydrochloric acid, and BisTris at 267 mM, 333 mM, or 400 mM (pH range from 6.0 to 6.5), plus 50 μM R6G and 0.4% PVP. TE: 200 mM serine, 10 mM $Ba(OH)_2$, and 0.4% PVP, pH 8.1. Voltage was 400 V. Injection plug contained 5 mm each of acetic acid (AA; ◇), MES (□), MOPS (×), HEPES (○), and tricine (TRI; +).

that tracers not focus often limits the use of overspeeders (e.g., we know of no fluorophore that can overspeed analytes such as chloride-containing residues from explosives[34]).

Interestingly, most experiments exhibited a signal overshoot at the MOPS−LE boundary (e.g., see Figure 4b). Such overshoots are common in ITP experiments.[14,35] Although previous model cases have captured similar overshoots[36,37] (which we confirm with our own predictions), our predictions with the current chemistries do not capture this. We know of no clear explanation for these overshoots and hypothesize that they may be due to finite chemical kinetic rate effects[38] not captured by current models (e.g., species crossing a zone boundary may require finite time to reach equilibrium). In any case, the overshoots do not seem to affect our ability to measure tracer intensity ratios or zone lengths, since we measured intensity values away from local peaks.

Next, we address the relation between measured analyte zone length and injected analyte concentration, $c_{a,\mathrm{inj}}$. Zone length prediction is discussed elsewhere[2,9] and in the Supporting Information. As expected from theory, and as shown in Figures 4 and 5, the dependence is linear in plateau mode ITP. The slope of the relation, however, depends on factors such as the LE composition. In Figure 5, we performed ITP with a very repeatable hydrodynamic injection (see Figure 3a) of a model analyte (MOPS) at various concentrations. We performed these experiments with either a high-concentration LE (hc-LE; 200 mM acetic acid, 400 mM BisTris) or a low-concentration LE (lc-LE; 100 mM acetic acid, 200 mM BisTris). The relative standard deviations for repetitions of the data plotted in Figure 5 ranged from 1% to 5%, averaging about 2.5%. Analyte zone lengths in the high hc-LE case are roughly twice those of the lc-LE case, as expected[19] (the slope coefficient of the linear regression lines are 120 ± 3 vs 64 ± 3 μm mM^{-1}, respectively). The hc-LE case shows a nonzero y-intercept (34 ± 21 μm), likely due to an impurity (not uncommon in ITP).[39] The near unity correlation coefficients show that calibration experiments enable accurate measurements of $c_{a,\mathrm{inj}}$. We note that, as discussed by Khurana and Santiago,[9] the minimum detectable zone length (i.e., created by the minimum detectable concentration) is of the order of the width of the adjacent ITP interfaces.

Analyte Identification. As discussed in the Theory section, tracer intensity measurements can assist in identifying unknown analytes. Accurate identification requires a well-characterized NFT. We often choose R6G for reasons mentioned above and because its fluorescence is relatively uniform between pH 2 and 10.[40,41] R6G has no pK_a's in this range, but it does show a tendency to adsorb to channel walls to a degree that slightly affects its mobility, especially above pH 2 and at ionic strength below 15 mM.[41,42] R6G exhibits self-quenching at >300 μM,[25] but fluorescence was approximately linear with concentration in our ranges of interest. Further, R6G is stable for over 6 months if stored in aqueous solution at pH ∼ 2.[42] We here model R6G as a fully ionized cation with limiting electrophoretic mobility (16.2 ± 0.7) × 10^{-9} m^2 V^{-1} s^{-1}, as measured by electrokinetic injection (see the Supporting Information for more details).

Figure 6 compares predicted with measured tracer intensities for 27 combinations of analyte and LE (including five analytes and six LEs). The predictions are based solely on known LE properties and predicted analyte effective mobility (based on fully ionized mobility, degree of dissociation, and ionic strength). The agreement between predictions and data shows that even the simple equations described in the Theory section above effectively collapse the data and yield fairly accurate solutions at high

(34) Prest, J. E.; Beardah, M. S.; Baldock, S. J.; Doyle, S. P.; Fielden, P. R.; Goddard, N. J.; Brown, B. J. T. *J. Chromatogr., A* **2008**, *1195*, 157–163.
(35) Bocek, P.; Gebauer, P.; Deml, M. *J. Chromatogr.* **1981**, *217*, 209–224.
(36) Mosher, R. A.; Thormann, W.; Bier, M. *J. Chromatogr.* **1985**, *320*, 23–32.
(37) Martens, J.; Reijenga, J. C.; Boonkkamp, J.; Mattheij, R. M. M.; Everaerts, F. M. *J. Chromatogr., A* **1997**, *772*, 49–62.
(38) Gebauer, P.; Bocek, P. *J. Chromatogr.* **1984**, *299*, 321–330.
(39) Prest, J. E.; Beardah, M. S.; Baldock, S. J.; Doyle, S. P.; Fielden, P. R.; Goddard, N. J.; Brown, B. J. T. *J. Chromatogr., A* **2008**, *1195*, 157–163.
(40) Arbeloa, F. L.; Gonzalez, I. L.; Ojeda, P. R.; Arbeloa, I. L. *J. Chem. Soc., Faraday Trans. 2* **1982**, *78*, 989–994.
(41) Chen, Z.; Tang, Y. J.; Xie, T. T.; Chen, Y.; Li, Y. Q. *J. Fluoresc.* **2008**, *18*, 93–100.
(42) Toptygin, D.; Packard, B. Z.; Brand, L. *Chem. Phys. Lett.* **1997**, *277*, 430–435.

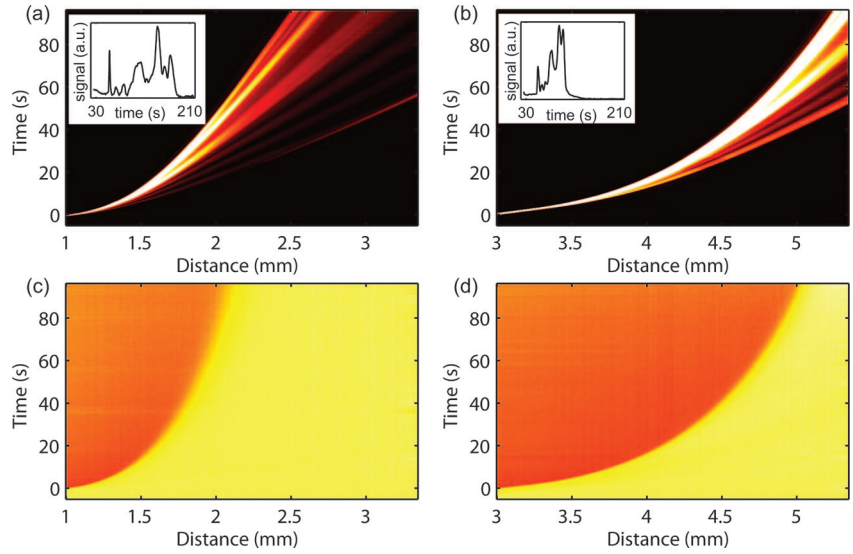

Figure 7. Fluorescence intensity vs time and separation channel distance in a tITP process. In the top plots, DNA is first isotachophoretically focused, as described in Figure 3b. ITP is disrupted by LE ions after the DNA zone passes a distance sd from the intersection. DNA then separates according to size. Bottom plots are visualizations of this TE-to-LE interface using a counterionic NFT. For sd = 1 mm (left column), ITP disruption is more abrupt and results in higher resolution (a). The corresponding NFT visualization (c) shows rapid deceleration and dispersion of the LE/TE interface. For sd = 3 mm (right column), ITP disruption is more gradual and we achieve markedly less resolution (b). The corresponding NFT visualization (d) shows a weaker deceleration and an LE/TE interface that persists over longer distances and times. Insets in panels a and b show fluorescence intensity vs time at points 3.5 and 5.5 mm from the intersection, respectively (including times not shown in the spatiotemporal plots). LE: 100 mM HCl, 200 mM Tris, 100 μM R6G, 10× Sybr Green, and 4% PVP, pH 8.1. TE: 38 mM glycine, 3.8 mM $Ba(OH)_2$, and 4% PVP, pH 9.0. Sample for panels a and c was 25 μg/mL of a 100 bp DNA ladder, dissolved in LE. Current was held constant at 1 μA.

intensity ratios. The model, however, somewhat overpredicts intensity values in the low intensity range, which is characterized by relatively low effective analyte mobilities (see eq 5). For example, the typical overprediction for acetic acid is roughly 1% but grows to 6% for MES, 21% for MOPS, 28% for HEPES, and 36% for tricine. We attribute most of the error to adsorption of R6G to channel walls, which we know to be most severe at the high pHs and low ionic strengths characteristic of slow anionic ITP zones. Another possible contributor to the disagreement is propagation of our uncertainties in analyte and/or LE pK_a and mobility data. For example, mobilities may be slightly altered from ideal values by our use of 0.4% PVP (we confirmed this with a limited number of supporting experiments).

Example Application to Optimization of a Complex ITP Assay. As explained in the Theory section, NFTs can be used to visualize and qualitatively study the dynamics of transient electrophoretic systems. Here, we demonstrate the use of a counterspeeder to monitor a transient ITP preconcentration followed by a capillary electrophoresis separation (tITP-CE), an important separation method.[30,43] As described in Figure 3b, we first preconcentrate a 100−1517 bp dsDNA ladder between a TE and an LE. The concentrated DNA zone electromigrates past a channel intersection in ITP mode, and at a given distance from the intersection (which we here define as the *switching distance*, sd) we change the applied current from the TE to the LE well.[12] LE ions enter the separation channel, overspeed TE ions, gradually disrupt ITP, and initiate CE separation in the PVP polymer sieving matrix.

In Figure 7a, we show a spatiotemporal plot of a typical tITP-CE separation of the DNA ladder with sd = 1 mm. The ITP-to-CE transition is not a fanlike expansion of straight sample traces from a single point. Instead, we see sample peak traces with pronounced curvature (deceleration) from which peaks gradually deviate. In Figure 7b, sd = 3 mm. Here, the ITP-to-CE process is markedly slower; some analytes remain focused in an ITP-like zone even after 1.75 mm. The switching distance clearly has a strong effect on the resolution of electropherograms, with shorter switching times providing much better resolution.

Visualization using an NFT visualization shows that the decrease in resolution with increased switching time is accompanied by very different dynamics in the ITP disruption process. Parts c and d of Figure 7 show counterspeeder (R6G) visualizations at conditions identical to those of Figure 7, parts a and b, respectively, except that the system does not contain DNA. (In Figure 7, parts a and b, DNA was present in relatively low-concentration peak mode and so should not have a strong effect on the LE and TE interface.) These visualizations show that the ITP interface does not disappear as LE ions begin to overspeed it. Instead, LE ions gradually dilute TE ions, creating a mixed TE/LE zone with an as-yet, self-sharpening front.[44] Longer switching distances result in a slower transition process and a TE-to-LE interface which persists over longer times and distances. This results in lower resolution for fixed separation length. We hope to further explore tITP optimization in a future report. For now, we conclude that the NFT visualization is efficacious in studying the dynamics of the LE-to-TE interface in this complex, peak mode DNA tITP process.

(43) Timerbaev, A. R.; Hirokawa, T. *Electrophoresis* **2006**, *27*, 323–340.
(44) Mikkers, F. E. P.; Everaerts, F. M.; Verheggen, T. *J. Chromatogr.* **1979**, *169*, 1–10.
(45) Hirokawa, T.; Gojo, T.; Kiso, Y. *J. Chromatogr.* **1986**, *369*, 59–81.

CONCLUSION

Fluorescent NFTs are a convenient and easy-to-implement alternative to classical ITP detection methods. NFT visualizations can be used to identify and quantify ITP zones, reveal information about analyte properties, and assist in identification of unknown analytes. We have described theoretically how NFT concentrations adapt in analyte zones and how multiple experiments can yield mobility and pK_a data. Further, we demonstrated the ability of NFTs to detect multiple analyte zones and to measure precisely initial analyte concentration. We showed also that experimentally measured tracer concentrations compare well with theory. In this work we primarily used R6G as a tracer but discussed the use, benefits, and drawbacks of other tracers. As an example application, we monitored a complex, transient ITP focusing step and subsequent DNA separation. We showed that the distance at which the ITP step was interrupted substantially impacted separation resolution and used NFT visualization to study the underlying ITP dynamics.

NFT visualization can be used with fairly standard point detectors and microscope CCD imaging systems. Significantly, CCD imaging enables real-time monitoring of ITP zones in both space and time. The technique is well-suited to detection of nonfluorescent analytes. The technique is likely also applicable to nonfluorescent NFTs, such as tracers with strong UV absorption or strong electrochemical signals.

In future work, we plan to explore other fluorescent tracers with a goal of identifying tracer chemistries with minimal wall adsorption, high quantum yield, and high effective mobilities in pH and ionic strength ranges of interest. We also plan to further study and optimize processes such as tITP-CE using NFTs.

ACKNOWLEDGMENT

R.D.C. was supported by a Stanford School of Engineering graduate fellowship and is currently supported by a Kodak fellowship. We gratefully acknowledge support from the Micro/Nano Fluidics Fundamentals Focus (MF3) Center funded by Defense Advanced Research Projects Agency (DARPA) MTO Grant No. HR0011-06-1-0050 and contributions from MF3 corporate members. We aslo gratefully acknowledge the support of the DARPA MTO sponsored SPAWAR Grant N66001-09-1-2007. We thank Moran Berocovici and Tarun Khurana for insightful discussions regarding ITP physics.

SUPPORTING INFORMATION AVAILABLE

Additional information as noted in text. This material is available free of charge via the Internet at http://pubs.acs.org.

Received for review December 19, 2008. Accepted February 6, 2009.

AC802698A